Hindawi
Advances in Civil Engineering
Volume 2024, Article ID 6616269, 15 pages
https://doi.org/10.1155/2024/6616269

Research Article

Landslide Susceptibility Mapping Using GIS and Bivariate Statistical Models in Chemoga Watershed, Ethiopia

Abinet Addis

Department of Civil Engineering, Debre Markos University, Debre Markos, Ethiopia

Correspondence should be addressed to Abinet Addis; abinetaddis2002@gmail.com

Received 6 June 2023; Revised 1 February 2024; Accepted 2 February 2024; Published 20 February 2024

Academic Editor: Gang Mei

This study aimed to map the landslide susceptibility in the Chemoga watershed, Ethiopia, using Geographic Information System (GIS) and bivariate statistical models. Based on Google earth imagery and field survey, about 169 landslide locations were identified and classified randomly into training datasets (70%) and test datasets (30%). Eleven landslides conditioning factors, including slope, elevation, aspect, curvature, topographic wetness index, normalized difference vegetation index, road, river, land use, rainfall, and lithology were integrated with training landslides to determine the weights of each factor and factor classes using both frequency ratio (FR) and information value (IV) models. The final landslide susceptibility map was classified into five classes: very low, low, moderate, high, and very high. The results of area under the curve (AUC) accuracy models showed that the success rates of the FR and IV models were 87.00% and 90.10%, while the prediction rates were 88.00% and 92.30%, respectively. This type of study will be very useful to the local government for future planning and decision on landslide mitigation plans.

1. Introduction

Landslide is a major natural hazard that poses a significant threat to human lives and infrastructure [1, 2]. Natural hazards such as landslides, flood, earthquake, and drought risk cannot be avoided completely but the processes and consequences can be mitigated [3, 4]. The Chemoga watershed, located in the northern part of Ethiopia, is prone to landslide hazards due to its steep slopes, rugged topography, and intense rainfall. The increasing population pressure and the rapid expansion of infrastructure have also contributed to the occurrence of landslides in the area [5, 6].

In Ethiopia landslides mostly manifest as rock fall, earth slide, debris and mudflow especially in the steep and hilly areas of the highlands greater than 1,500 m altitude [7, 8]. According to Meten et al. [9], from 1960 to 2010 about 388 people are reported dead, 24 injured, and a great deal of agricultural lands, houses, and infrastructures were affected. The occurrence of landslides is an extremely complex phenomenon which depends upon various factors such as geologic structure, lithological association, topography, rainfall, earthquake, and human activity [10]. One of the most widely used approaches to reduce the landslide damages is preparing a landslide susceptibility mapping using suitable models and selecting the effective conditioning factors [11, 12]. Over the last decades, many studies utilized used different models to prepare landslide susceptibility mapping. These models include the frequency ratio (FR) model [2, 4, 13–18]. Frequency and Shannon entropy models [19–24], weights of evidence model [12, 25–29], and Shannon entropy model [11, 30–33]. Landslide susceptibility models based on the bivariate frequency and weights of evidence models [34] and FR and information value (IV) models [1, 10, 35], machine learning models [36, 37], and deep learning models [38, 39] have been developed. With the development of Geographic Information System (GIS), other researchers have used bivariate FR and multivariate logistic regression models [40–44] to help in the calculation and visualization of the cumulative effects of conditioning factors on landslides.

In this study, we aimed to develop a landslide susceptibility map using GIS and bivariate statistical models in the Chemoga watershed, Ethiopia. We collected landslide inventory data through field surveys and prepared various thematic layers such as slope, elevation, aspect, curvature, topographic wetness index (TWI), normalized difference vegetation index,

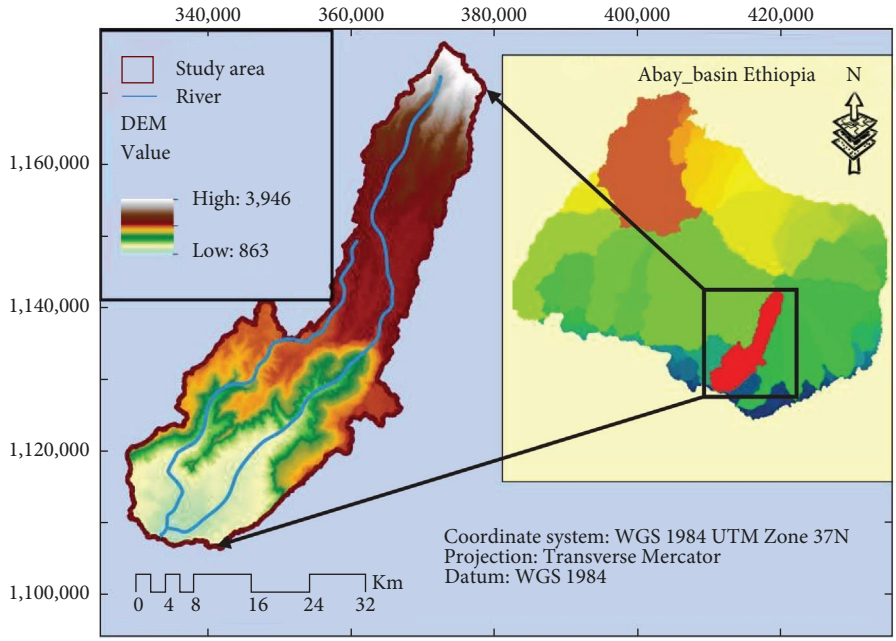

Figure 1: Location map of study area.

road, river, land use, rainfall, and lithology from the digital elevation model (DEM) and satellite imagery. Two bivariate statistical models, namely, FR and IV, were used to analyze the relationships between the landslide occurrences and the thematic layers. The accuracy of the models was evaluated using a validation dataset.

The results of this study can provide valuable information for land use planning and management in the Chemoga watershed. The development of a landslide susceptibility map can help in identifying areas that are prone to landslide hazards and prioritizing mitigation measures to reduce the risk of landslide disasters.

2. Materials and Methods

2.1. Description of the Study Area. The Chemoga watershed is located in the upper Abay River basin Ethiopia with an area 1,414.85 km^2. According from UTM coordinate system (zone 37N), the location of watershed is approximately between longitudes 330,000–380,000 m E and latitude 1,110,000–1,170,000 m N and topographically, the altitude ranges from 863 to 3,946 m, shown in Figure 1. Topographically, the altitude ranges from 863 to 3,946 m and the slope angle varies from 0° to 67°. In terms of land use, most of the watershed is covered by scrub/shrub and crop lands. The study area receives high amount of rainfall during the summer season. Based on Ethiopian National Metrological Agency, the average recorded annual precipitation and temperature of the area was 1,376 mm and 16.95°C, respectively.

2.2. Data Source and Methodology. In this study, I used both primary and secondary data. The primary data were collected from field survey and observation and the secondary data were acquired from governmental and nongovernmental institutions, journals, internet, and other documents. The main data used for this study were sentinel-2 images and 30 m DEM of the area, Google earth imagery and topographical map of the area. The data layer of land use and NDVI were derived from Sentinel-2 images and DEM data used to create the slope, elevation, aspect, curvature, and TWI data layers and their extents through spatial analysis tools. The data of annual rainfall were obtained from the National Meteorological Agency of Ethiopia. The main road and river were digitized from the topographical map of Ethiopia and the geological map was used to create the lithology layer of the study area. All the data layers have been constructed and combined in ArcGIS 10.4 tool. Accordingly, the FR and IV models were used to generate elaborative landslides susceptibility map. The conditioning factors considered, their format and sources is presented in Table 1, while the methodological workflow is shown in Figure 2.

2.3. Landslide Inventory Map. Landslide inventory mapping is the systematic mapping of existing landslides in a region using various techniques such as field survey, aerial photographs or Google earth imagery interpretation, satellite image interpretation, and literature search technical and scientific reports, governmental reports, and the interview of experts [45, 46]. In this study, the landslides inventory map which has a total of 169 individual landslide locations was generated according to the integration of different data sources such as Google earth imagery digitized into points and field surveys, i.e., GPS points (period between 2016 and 2022). Landslide types in the study area include rockslide, soil slide, debris flow, earth flow, rock fall, and rock toppling. Though there is no specific rule for defining how landslide occurrence will be allocated into training and validation data sets [47], usually research work has been done by using 70% of landslides events as training data sets and the rest 30% for validation of the output model [11, 14, 48]. In this study, 118

Table 1: Type of conditioning factors, format, and source.

Type conditioning factors	Format	Source
Slope, elevation, aspect, curvature and TWI	Raster (30 m)	Derived from of DEM image (2021)
Road and river	Vector (scale 1 : 500,000)	Digitized from the study area of topographic map, Ethiopian Mapping Agency, Addis Ababa, Ethiopia
Land use and NDVI	Raster (30 m)	Analyzed from Sentinel-2 images in the USGS (2021)
Lithology	Vector (scale 1 : 500,000)	Digitized from the study area of geological map, Minister of Water and Energy, Addis Ababa, Ethiopia
Rainfall	Vector	Interpretation of Ethiopian National Metrological Agency, Addis Ababa (1990–2021)
Landslide inventory		Digitized from Google earth imagery and field survey

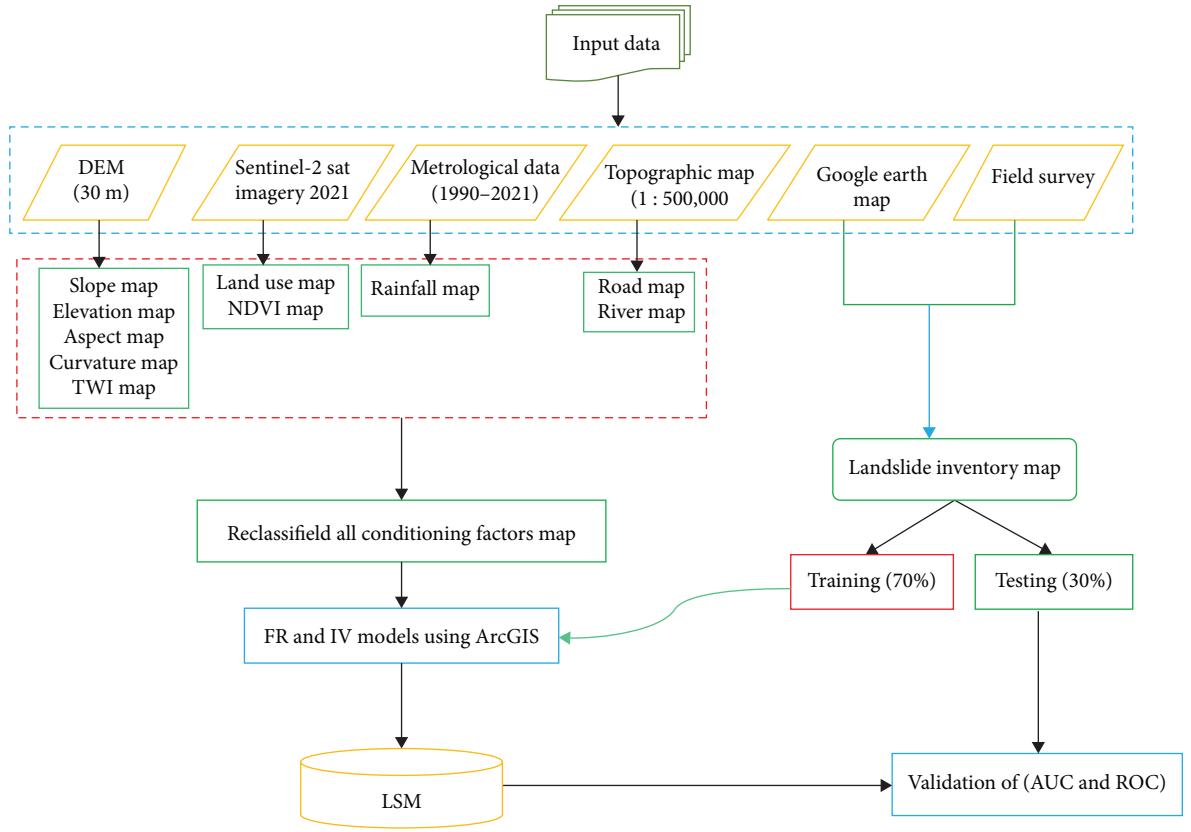

Figure 2: Workflow of the methodology.

(70%) of the landslides inventory data were used for model training and the remaining 51 (30%) of the landslides inventory data were used for validation.

2.4. Landslide Conditioning Factors. To identify landslide occurrence conditioning factors is a very complex phenomenon, because there is no standard rule to select which factor to be used [49]. In this study, 11 conditioning factors were selected based on the literatures, effectiveness, availability of data, and the relevance with respect to land slide occurrence [23]. These conditioning factors are slope, elevation, aspect, curvature, TWI, NDVI, road, river, land use, rainfall, and lithology. Each factor was converted to a raster format and was classified based on Jenks natural breaks method in ArcGIS, shown in Figure 3.

In landslide susceptibility studies, slope is considered one of the major contributing factor [21, 50]. According to the importance of slope contribution factor landslide occurrence, the slope data were classified into five classes. With increase in slope angle, the possibility of landslide occurrence increases [19, 51, 52]. Elevation is an important conditioning factor in landslide susceptibility mapping and it also impacts the environmental conditions on slopes such as human activity, vegetation, soil moisture, and climate [53, 54]. Curvature has an important role in the surface runoff and ground infiltration thus affects the erosion of the surface and ground

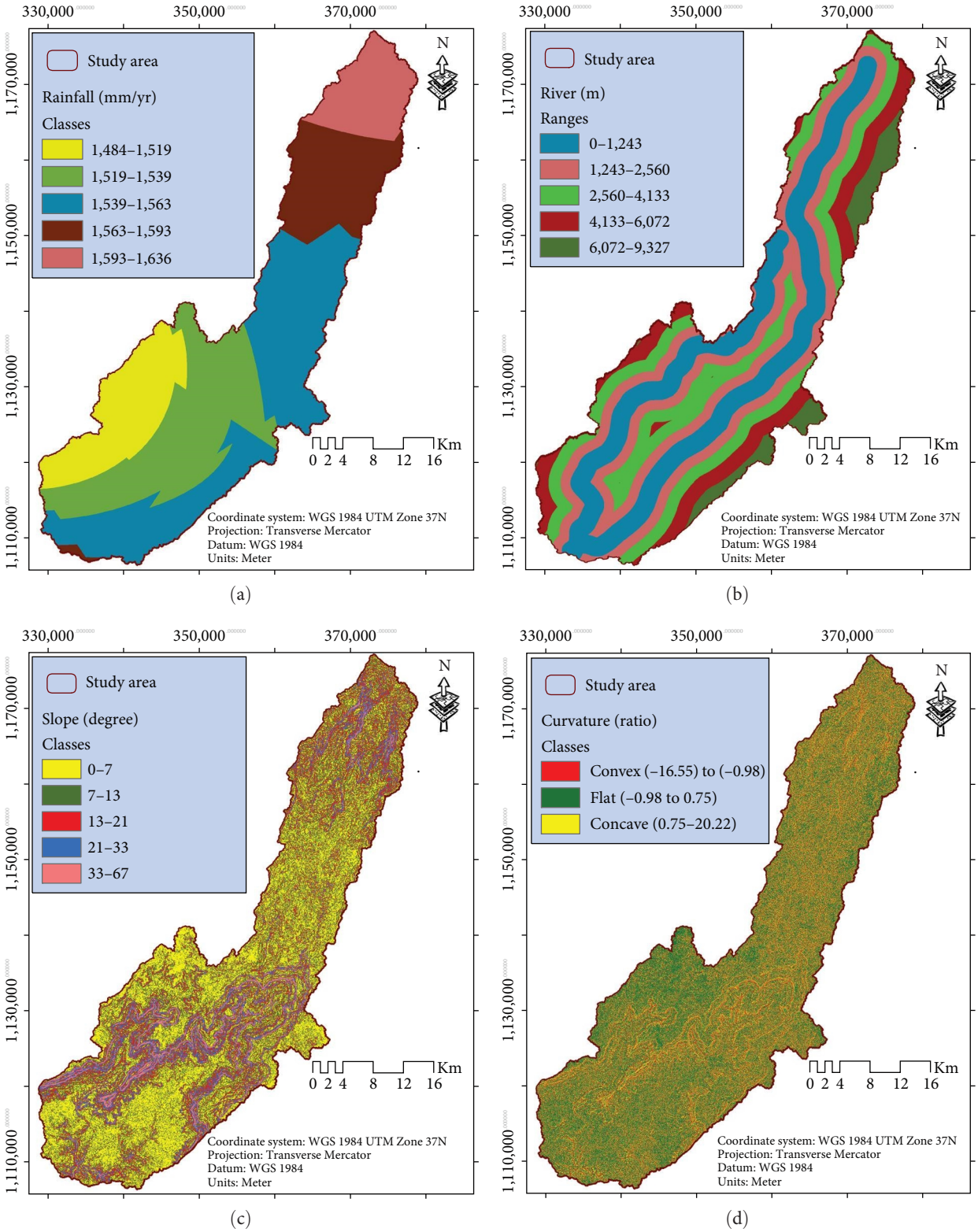

Figure 3: Continued.

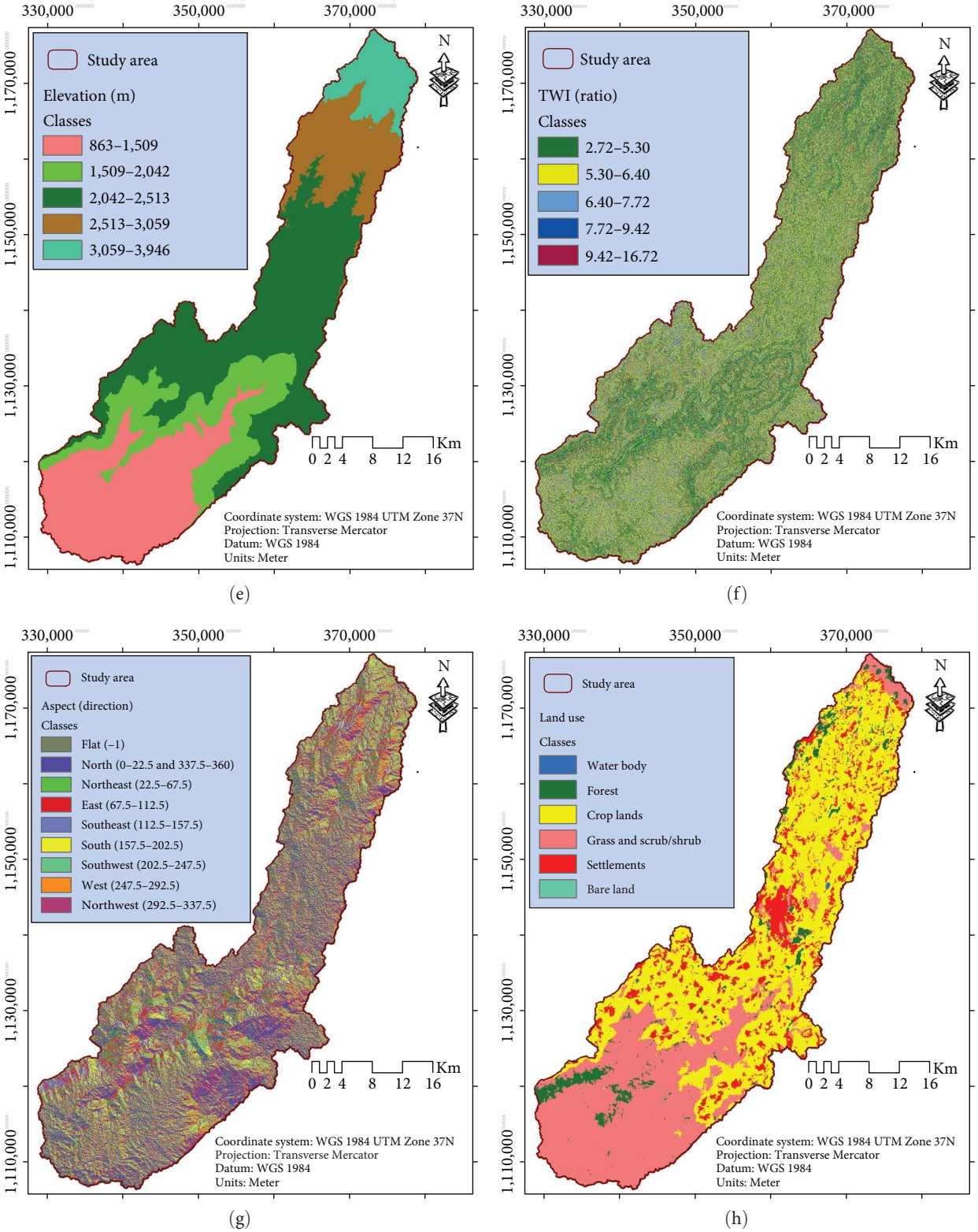

Figure 3: Continued.

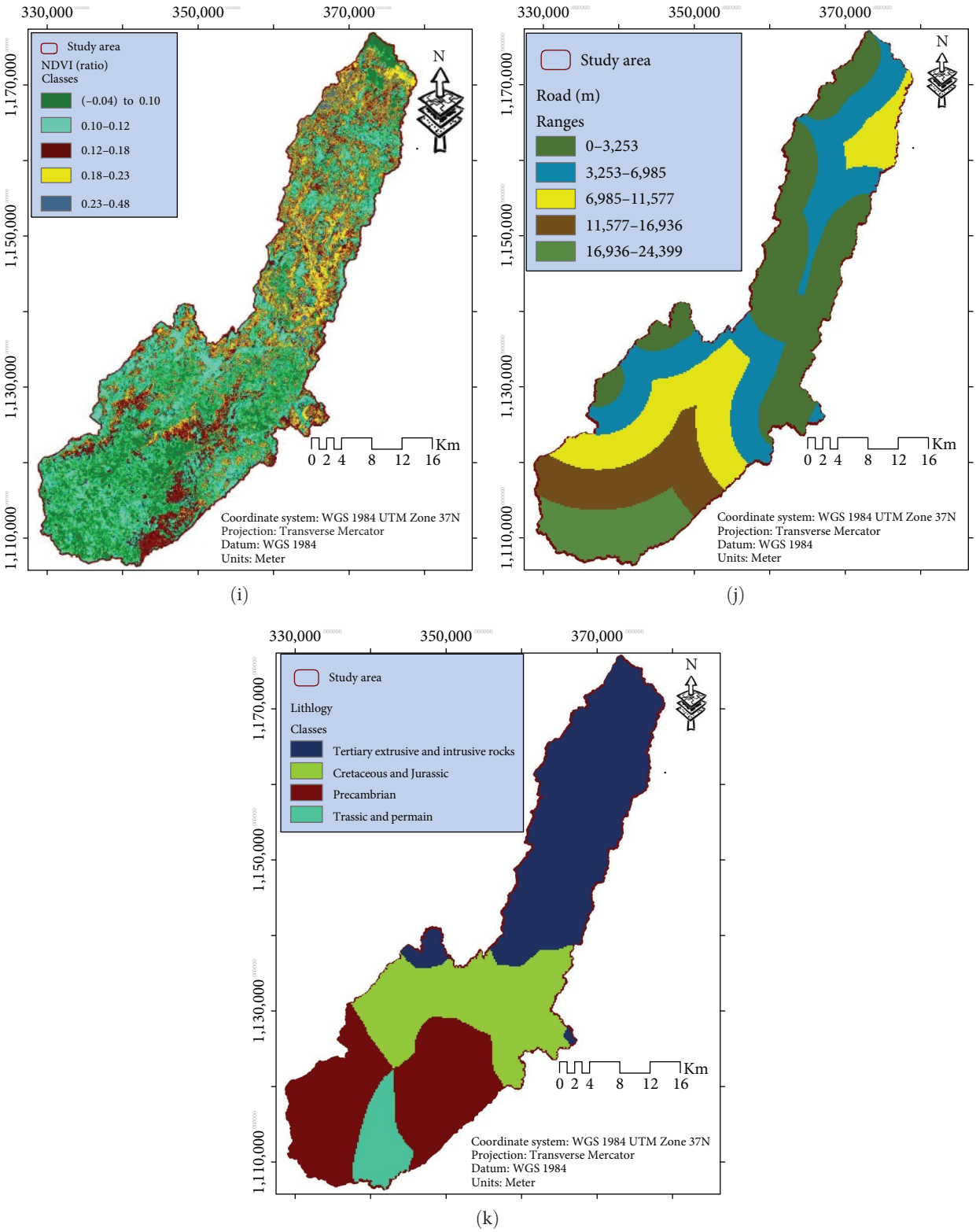

Figure 3: Landslide conditioning factors; (a) rainfall map, (b) river map, (c) slope map, (d) curvature map, (e) elevation map, (f) TWI map, (g) aspect map, (h) land use map, (i) NDVI Map, (j) distance from road, and (k) lithology map.

water condition of the region [17]. The curvature map was classified into concave (negative), convex (positive), and flat (zero) surfaces. In the case of curvature, the more negative the value, the higher the probability of landslide occurrence [29]. Aspect represents the direction that a slope faces [53]. Slope aspect affects erosion, surface evaporation, desertification, solar heating and surface weathering, thus affecting the occurrence of landslides [50, 55]. TWI is among one of the

important factors responsible for the landslide, which can quantitatively display the control of terrain on the spatial distribution of soil moisture, is a widely used terrain attribute. The TWI conditioning factor was obtained from DEM with 30 m spatial resolution by Equation (1) to express as follows:

$$\mathrm{TWI} = \mathrm{Ln}(A_s/\tan\beta), \tag{1}$$

where A_s is the specific catchment area (m^2/m) and β is slope angle in degrees [56]. TWI is used to measure topographic control of hydrological procedures [57]. Rainfall is considered to be one of the landslides occurrences conditioning factor. Rainfall map was prepared using five station locations in the study area through the IDW interpolation method of annual average precipitation (1990–2021). Road is one of the most effective factors on landslide occurrence [1]. Road construction near the hillside may lead to changes in the natural conditions of areas. River networks plays an important role in landslide occurrence factor closely to surface water. The NDVI conditioning factor was obtained from Sentinel-2 satellite imagery with 30 m spatial resolution by Equation (2) to express as follows:

$$\mathrm{NDVI} = \frac{\mathrm{IR\text{-}R}}{\mathrm{IR} + \mathrm{R}}, \tag{2}$$

where IR is the infrared and R is the red bands of the electromagnetic spectrum. NDVI values between −1.0 and 1.0, where any negative values are mainly generated from clouds, water, and snow and values near zero are mainly generated from rock and bare soil and the positive value indicates that the ground is covered by vegetation. Land use is an important conditioning factor that affects the occurrence of landslides. The map of land use was derived from Sentinel-2 satellite imagery, by using a supervised classification technique and classified in to six classes. The study area is predominantly covered with the cropland and scrubs. The lithology also classified into four classes and the dominant lithology is tertiary extrusive and intrusive rocks in the study area.

2.5. Landslide Susceptibility Modeling

2.5.1. Frequency Ratio (FR) Model. FR is one of the most widely adopted and popular methods for landslide susceptibility assessment [14, 16, 58]. The FR is the ratio of the area where landslides occurred in the total study area and also is the ratio of the probabilities of a landslide occurrence to a non-landslides occurrence for a given attribute [59, 60]. Generally, a greater ratio indicates a stronger relationship between a conditioning factor and landslide and vice versa. FR value is greater than 1, it indicates a high probability of landslide occurrence, and a value less than 1 indicates a low relationship between probabilities of landslide occurrence. The landslides susceptibility map (LSM) can be calculated by summing the FR of all of the factors considered Equation (3) as follows:

$$\begin{aligned}\mathrm{LSM} &= \sum_{j=1}^{n} \mathrm{FR} \\ \mathrm{LSM} &= \big(\mathrm{FR}_{\mathrm{slope}} + \mathrm{FR}_{\mathrm{elevation}} + \mathrm{FR}_{\mathrm{aspect}} + \mathrm{FR}_{\mathrm{land\,use}} \\ &\quad + \mathrm{FR}_{\mathrm{curvature}} + \mathrm{FR}_{\mathrm{road}} + \mathrm{FR}_{\mathrm{river}} + \mathrm{FR}_{\mathrm{NDVI}} \\ &\quad + \mathrm{FR}_{\mathrm{TWI}} + \mathrm{FR}_{\mathrm{rainfall}} + \mathrm{FR}_{\mathrm{Lithology}}\big),\end{aligned} \tag{3}$$

where LSM is landslide susceptibility map and FR represents for each factor type or class, n is the number of factors. The FR can be obtained by Equation (4) as follows:

$$\mathrm{FR} = \left[\frac{N''\mathrm{pix}''(\mathrm{SX}_i)/\sum_{i=1}^{m}\mathrm{SX}_i}{N''\mathrm{pix}''(\mathrm{X}_j)/\sum_{j=1}^{n}N''\mathrm{pix}''(\mathrm{X}_j)}\right], \tag{4}$$

where the number of landslide pixels in class i of the factor X is represented by N_{pix} (SX_i); the total number of pixels within factor X_j is represented by $N_{\mathrm{pix}}(X_j)$; m is the number of classes in factor X_i; and n is the total number of factors in the study area [60].

2.5.2. Information Value (IV) Model. The IV model is a bivariate statistical approach that objectively assesses landslide susceptibility using information theory, providing an advantage in accurately identifying areas at risk of landslides and the model was originally proposed by [61] and later slightly modified by [46]. The information value model is used to evaluate the spatial relationship between the conditioning factor classes and the probability of landslide occurrence. Generally, the higher value of IV model corresponds to the stronger relationship between the probability of landslide occurrence and the conditioning factor class. IV value is greater than 0 indicates a high probability of landslide occurrence, and a value less than 0 indicates a low relationship between the probabilities of landslide occurrence. Therefore, the LSM for each pixel was computed by summing the information values of each factor class as follows:

$$\begin{aligned}\mathrm{LSM} &= \sum_{i=1}^{n} \mathrm{IV}i \\ \mathrm{LSM} &= \big(\mathrm{IV}_{\mathrm{Slope}} + \mathrm{IV}_{\mathrm{Elevation}} + \mathrm{IV}_{\mathrm{Aspect}} + \mathrm{IV}_{\mathrm{Land\,use}} \\ &\quad + \mathrm{IV}_{\mathrm{Curvature}} + \mathrm{IV}_{\mathrm{road}} + \mathrm{IV}_{\mathrm{river}} + \mathrm{IV}_{\mathrm{NDVI}} \\ &\quad + \mathrm{IV}_{\mathrm{TWI}} + \mathrm{IV}_{\mathrm{Rainfall}} + \mathrm{IV}_{\mathrm{Lithology}}\big),\end{aligned} \tag{5}$$

where LSM is the landslide susceptibility map and IVi is the information value each factor class, n is the number of factors. IV was applied, and the weights were assigned to each class of each conditioning factor. The information value (IV) can be calculated using the following formula [61]:

$$\begin{aligned}\mathrm{IV} &= \log(\mathrm{Conditional\,probability}/\mathrm{prior\,probability}) \\ &= \log\left[\frac{\mathrm{Nsl}''\mathrm{pix}''/\mathrm{Nc}''\mathrm{pix}''}{\mathrm{Nts}''\mathrm{pix}''/\mathrm{Nta}''\mathrm{pix}''}\right],\end{aligned} \tag{6}$$

where Nslpix is a number of landslide pixels in a given class, Ncpix is the number of pixels in a given class, Ntspix is a total

number of landslide pixels in the study area, and Ntapix is a total number of pixels in the study area.

3. Results and Discussion

3.1. Application of Frequency Ratio (FR) Model. FR was measured for each class of every landslide conditioning factor by dividing the landslide occurrence ratio by the area ratio. The results of the FR model for each of the classes of effective factors are shown in Table 2. In general, the FR value of 1 indicates the average correlation between landslide occurrence and effective factors. A FR value greater than 1 indicates a high likelihood of landslide occurrence, while a FR value less than 1 indicates a low likelihood of landslide occurrence [47]. The analysis of FR for the relationship between landslide occurrence and slope degree indicate that class 33°–67°, the highest FR value of 9.27 among the other classes of slope degree. The remaining classes of slope have low probabilities of landslide occurrence. In the study area, it was observed that the probability of landslide occurrence increased with slope gradient up to a certain extent, and then decreased, consistent with results from other literature studies [20]. This is because higher slope values increase the effects of gravity and shear stress [46]. The relationship between landslide occurrence and elevation indicated that the range between 1,509 and 2,042 m, with a FR value of 2.78, had a high probability of landslide occurrence in the study area. The elevation ranges between 863–1,509, 2,042–2,513, 2,513–3,059, and 3,059–3,946 m, have lower FR values (0.28, 0.99, 0.41, and 0.53, respectively), indicating low probabilities of landslide occurrence. Commonly, as the elevation increases, the probability of landslide occurrence increases. The aspect factor classes with the highest abundance of landslide occurrence probability were east facing (FR = 1.03), south east facing (FR = 1.60), south facing (FR = 1.24), south west facing (FR = 1.42), west facing (FR = 1.24), and northwest facing (FR = 1.04), indicating a high probability of landslide occurrence in these areas. However, the remaining aspect classes have lower abundance of FR value less than 1, it indicates that a low probabilities of landslide occurrence. Considering the land use, results show that the water body, forest area, grass and scrub/shrub and bare land use types have values of FR (2.07, 1.50, 1.54, and 22.92, respectively), implying a high probabilities of landslide occurrence. The highest FR value of bare land are due to its exposure to erosion and soil moisture [41]. In the case of curvature factor classes of concave (−16.55 to (−0.98)) and convex (0.75–20.22), have the highest value of FR (1.39 and 1.38), respectively, indicating a high probabilities of landslide occurrence. The other curvature class of flat slope has a low FR value (0.70), indicating that a low probabilities of landslide occurrence. Distance from the road classes 6,985–11,577 m with a value of FR (2.05), has the greatest impact on landslide coherence. Commonly, the landslide frequency increases as the distance from roads decreases. Therefore, the existing road and the on-going constructions disturb the stability of slope there by increasing the probability of landslide occurrence [19, 20]. According to Guzzetti [62], the landslides probability decreases with the increasing distance from river networks. In this study area, distance from river network between 2,560–4,133 m exerts the highest influence on landslide occurrence. The reason is that permanent rivers are the main source of moisture for landslide occurrence. In the NDVI, the FR value is greater than one, where the NDVI classes −0.04 to 0.10 and 0.23–0.48, indicating a high probabilities of landslides occurrence. This range of NDVI values represents the bare land, built up areas and scrubs. However, the remaining NDVI classes have low FR value less 1. The relationship between TWI landslide probabilities showed that the range of TWI value from 2.72 to 5.30 has the highest FR (1.98). With regard to the rainfall, the range 1,484–1,519, 1,519–1,539, and 1,539–1,563 mm/yr have higher FR value than the other classes contributing more to landslide occurrence. Lithology factor classes are the most abundance on Precambrian (FR = 1.89) and Triassic and permain (FR = 2.29), indicating that a high probabilities of landslides occurrence. However, the remaining lithology classes have the lowest abundance of FR value less than 1, it indicates that a low probabilities of landslides occurrence.

3.2. Application of Information Value Model. The information value of each conditioning factor was calculated through Equation (5), and the spatial relationship between each conditioning factors and flood occurrence is shown in (Table 2). If the factor class of IV value is negative, there is a low likelihood of landslide occurrence. On the other hand, if the value is positive, there is a high-probability value is landslide occurrence [46]. The slope indicate that 33°–67° is highly prone to landslide having the highest IV value of 0.967, whereas the flat slope shows less probability. The occurrence of landslides tends to increase with higher slopes and decrease with lower slopes. The elevation factor indicate that the class 1,509–2,042 m (IV = 445), has a high probabilities of landslide occurrence and all other classes have very low impact. Generally, landslides mostly occurred on the higher area. But in this study, the landslides occurred in the lower area. The aspect conditioning factor classes have the lowest abundance on flat facing (IV = −0.534), north (IV = −0.434), and northeast (IV = −0.166) indicating a low probabilities of landslide occurrence. The remaining categories with positive IV values indicate a high probability of landslide occurrence. In terms of curvature, the flat class has the lowest IV value (−0.156) indicating a low probability of landslide occurrence, while the convex and concave classes have higher IV values (0.142 and 0.139, respectively), indicating a high probability of landslide occurrence. Distance from the road factor also shows that the class between 6,985–11,577 m has the highest IV value (0.312), indicating a high probability of landslide occurrence. The distance to river factor has a high IV value (0.178) for subclass 2,560–4,133 m, while the remaining subclasses have low IV values indicating a low probability of landslide occurrence. NDVI classes −0.04 to 0.10 and 0.23–0.48 have positive IV values indicating a high probability of landslide occurrence, while the remaining NDVI classes have negative IV values

Table 2: Spatial relationship between each conditioning factors and landslide occurrence using FR and IV models.

Conditioning factors	Classes	Class pixels	Class pixels (%)	Landslide pixels	Landslide pixels (%)	FR	IV
TWI	2.72–5.30	323,931	25.08	1594	49.64	1.98	0.297
	5.30–6.40	494,455	38.28	830	25.85	0.68	−0.171
	6.40–7.72	268,130	20.76	440	13.7	0.66	−0.18
	7.72–9.42	142,058	11	260	8.1	0.74	−0.133
	9.42–16.72	63,073	4.88	87	2.71	0.55	−0.256
Land use	Water body	582	0.05	3	0.09	2.07	0.317
	Forest	59,977	4.64	223	6.94	1.5	0.175
	Crops land	639,319	49.5	1,217	37.9	0.77	−0.116
	Grass/scrub/shrub	451,440	34.95	1730	53.88	1.54	0.188
	Settlements	139,820	10.82	9	0.28	0.03	−1.587
	Bare land	509	0.04	29	0.9	22.92	1.36
NDVI (ratio)	(−0.04) to 0.10	231,989	17.96	1,007	31.36	1.75	0.242
	0.10–0.12	458,792	35.52	945	29.43	0.83	−0.082
	0.12–0.18	367,141	28.42	692	21.55	0.76	−0.12
	0.18–0.23	180,380	13.97	410	12.77	0.91	−0.039
	0.23–0.48	53,345	4.13	157	4.89	1.18	0.073
Road (m)	0 −3,253	392,519	30.39	752	23.49	0.77	−0.112
	3,253–6,985	327,932	25.39	641	20.02	0.79	−0.103
	6,985–11,577	264,136	20.45	1,342	41.92	2.05	0.312
	11,577–16,936	174,099	13.48	380	11.87	0.88	−0.055
	16,936–24,399	133,032	10.3	86	2.69	0.26	−0.584
Rainfall (mm/yr)	1,484–1,519	196,729	15.23	647	20.15	1.32	0.122
	1,519–1,539	331,512	25.67	946	29.46	1.15	0.06
	1,539–1,563	438,126	33.92	1,343	41.82	1.23	0.091
	1,563–1,593	195,465	15.13	50	1.56	0.1	−0.988
	1,593–1,636	129,815	10.05	225	7.01	0.7	−0.157
River (m)	0–1,243	384,766	29.79	949	29.55	0.99	−0.003
	1,243–2,560	363,147	28.12	787	24.51	0.87	−0.06
	2,560–4,133	304,347	23.57	1,139	35.47	1.51	0.178
	4,133–6,072	160,917	12.46	306	9.53	0.76	−0.116
	6,072–9,327	78,320	6.06	30	0.93	0.15	−0.812
Slope (degree)	0–7	447,188	34.62	263	8.19	0.24	−0.626
	7–13	449,831	34.83	467	14.54	0.42	−0.379
	13–21	244,633	18.94	607	18.9	1.00	−0.001
	21–33	107,403	8.32	892	27.78	3.34	0.524
	33–67	42,592	3.3	982	30.58	9.27	0.967
Curvature (ratio)	Convex (−16.55 to (−0.98)	248,830	19.26	858	26.72	1.39	0.142
	Flat (−0.98 to 0.75)	721,286	55.84	1,253	39.02	0.7	−0.156
	Concave (0.75–20.22)	321,531	24.89	1,100	34.26	1.38	0.139
Elevation (m)	863–1,509	334,549	25.9	235	7.32	0.28	−0.549

Table 2: Continued.

Conditioning factors	Classes	Class pixels	Class pixels (%)	Landslide pixels	Landslide pixels (%)	FR	IV
	1,509–2,042	216,355	16.75	1,497	46.62	2.78	0.445
	2,042–2,513	482,883	37.39	1,190	37.06	0.99	−0.004
	2,513–3,059	169,167	13.1	172	5.36	0.41	−0.388
	3,059–3,946	88,693	6.87	117	3.64	0.53	−0.275
	flat (−1)	82,464	6.38	60	1.87	0.29	−0.534
	North (0–22.5 and 337.5–360)	213,107	16.5	195	6.07	0.37	−0.434
	Northeast (22.5–67.5)	123,845	9.59	210	6.54	0.68	−0.166
	East (67.5–112.5)	151,109	11.7	388	12.08	1.03	0.014
Aspect (direction)	Southeast (112.5–157.5)	158,025	12.23	629	19.59	1.6	0.204
	South (157.5–202.5)	131,648	10.19	407	12.68	1.24	0.095
	Southwest (202.5–247.5)	142,068	11	502	15.63	1.42	0.153
	West (247.5–292.5)	146,211	11.32	449	13.98	1.24	0.092
	Northwest (292.5–337.5)	143,170	11.08	371	11.55	1.04	0.018
	Tertiary extrusive and intrusive rocks	497,273	38.58	438	10.22	0.27	−0.576
Lithology	Cretaceous and Jurassic	323,705	25.11	804	18.77	0.75	−0.126
	Precambrian	391,465	30.37	2,460	57.42	1.89	0.278
	Triassic and permain	76,620	5.94	582	13.59	2.29	0.360

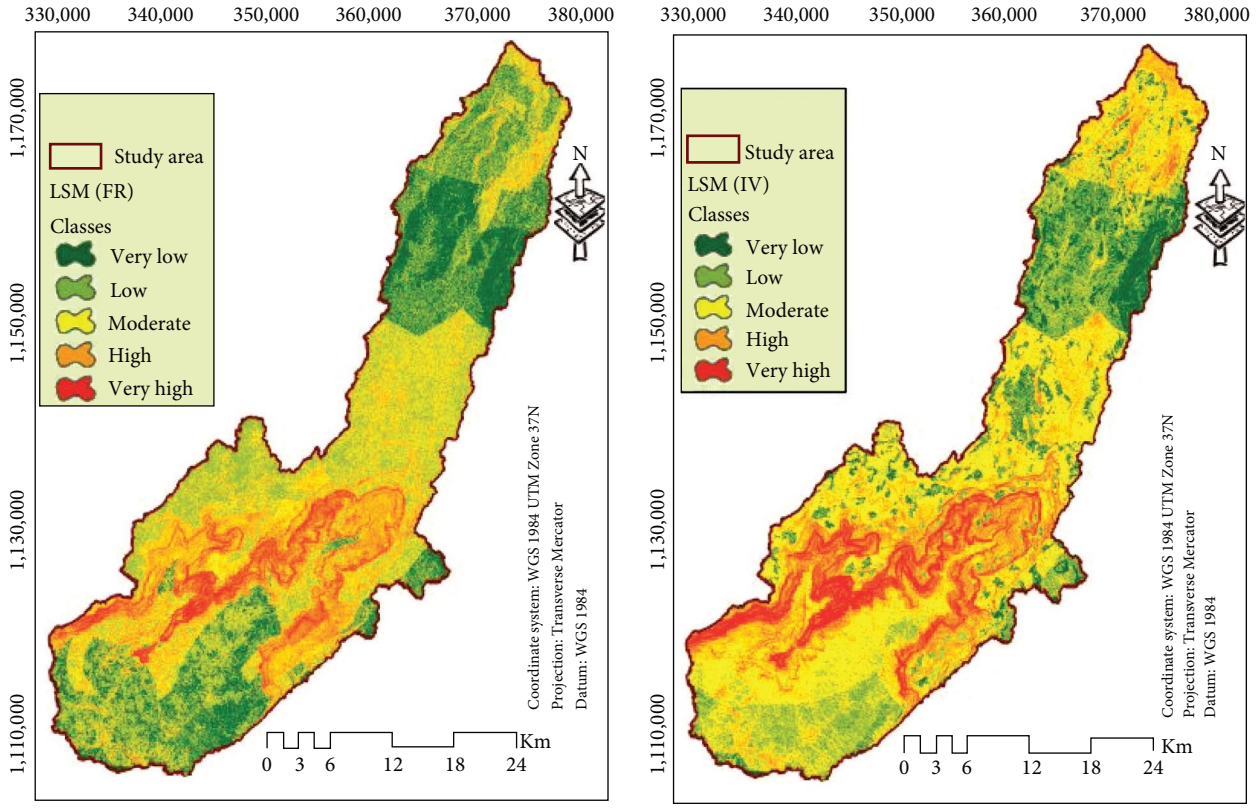

Figure 4: Landslide susceptibility map using: (a) frequency ratio (FR) and (b) information values (IV) models.

Table 3: Landslide susceptibility classes and summery of FR and IV models.

Landslide susceptible classes	FR model			IV model		
	Range	Area (km^2)	Area (%)	Range	Area (km^2)	Area (%)
Very low	14–27	245.62	17.36	−5.59 to (−2.35)	129.73	9.17
Low	27–35	450.80	31.86	−2.35 to (−1.34)	341.72	24.15
Moderate	35–43	383.44	27.10	−1.34 to (−0.45)	492.47	34.81
High	43–54	247.59	17.50	−0.45 to 0.71	316.20	22.35
Very high	54–81	87.40	6.18	0.71 to 3.91	134.72	9.52

indicating a low probability of landslide occurrence. TWI classes 2.72–5.30 also have a positive IV value (0.297), indicating a higher landslide occurrence. In terms of land use, settlements and crops can reduce the likelihood of landslide occurrence, while forest area, water body, grasses, and bare land have a high impact on landslide occurrence. The relationship between average annual rainfall and landslide occurrence shows that classes with higher rainfall (1,484–1,519, 1,519–1,539, and 1,539–1,563 mm/yr) have positive IV values, indicating a high probability of landslide occurrence, while the other classes have negative IV values indicating a low probability of landslide occurrence. The other important conditioning factor is lithology in this study. Lithology factor classes are the most abundance on Precambrian and Triassic and per main (IV = 0.278) and Triassic and permain (IV = 0.360), indicating a high probabilities of landslide occurrence. However, the remaining lithology classes have negative IV value which indicates a low probabilities of landslide occurrence.

3.3. Landslide Susceptibility Maps. The calculated FR values for each pixel indicate the relative susceptibility to landslide occurrence. The higher pixel values of LSM have the higher landslide susceptibility while the lower pixel values have lower susceptibility. The LSM values for the FR and IVs models in the study area ranges varies from 14 to 81 (Figure 4(a)) and −5.59 to 3.91 (Figure 4(b)), respectively. These values were classified into five susceptibility classes of very low, low, moderate, high, and very high susceptibility in both models using the geometrical interval method for visual interpretation, shown in (Table 3).

3.4. Validation of Landslide Susceptibility Maps. The FR and IV models were validated to check their reliability and

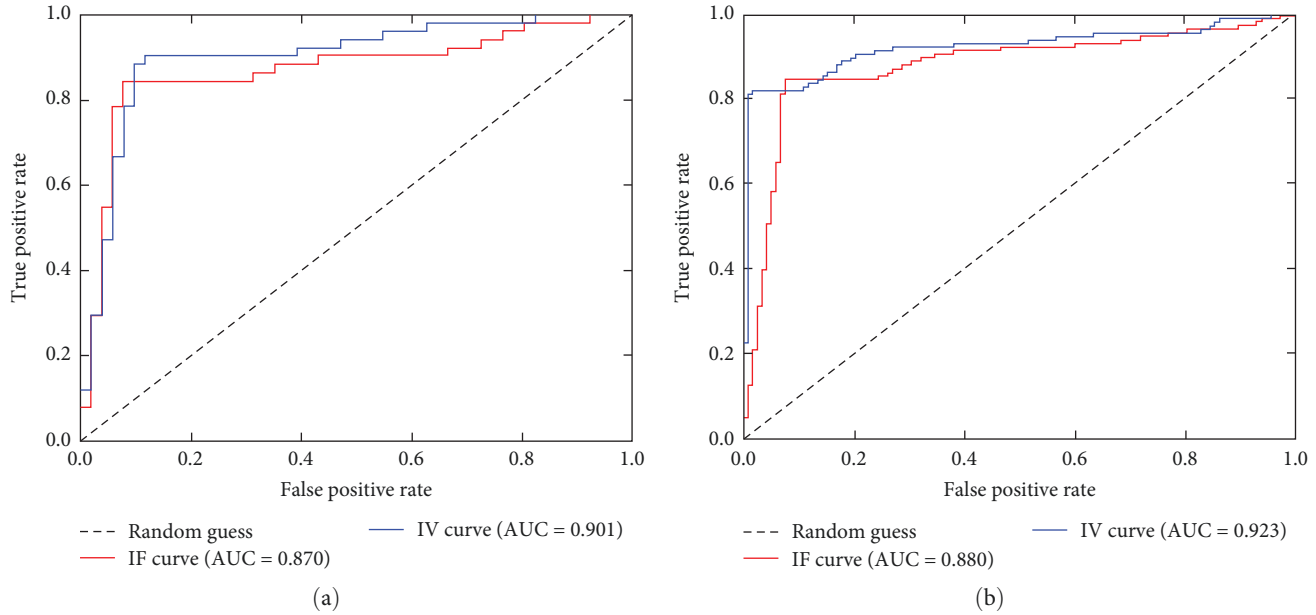

Figure 5: The AUC of success rate curve: (a) and prediction rate curve, (b) both FR and IV models.

performance. In the present study, the performance of the LSM produced by FR and IV models was evaluated using area under the curve (AUC). The AUC is the measure that indicates the accuracy of the landslide susceptibility maps by creating success and prediction rate curves [63]. The success rate curve represents the model fitness to the existing landslide. The prediction rate curve indicates the model efficiency to predict future landslide [47]. The AUC rate curves were drawn through the x-axis both the training and validation landslides (true positive rate) and y-axis (false positive rate). The total AUC value can be utilized as a qualitative measure to determine the accuracy of the susceptibility map, where a larger value indicates a higher level of accuracy achieved. The AUC value ranges from 0.5 to 1.0 are used to evaluate the accuracy of the model [63]. The qualitative relationship between AUC and prediction accuracy can be classified as follows; excellent (0.9–1.0); very good (0.8–0.9); good (0.7–0.8); average (0.6–0.7), and fair (0.5–0.6), [63]. If AUC value is close to 1.0, then the model will have ideal performance, where as a value is equal or less than 0.5, then the model will have poor performance [64]. The results indicated that the AUC values for the success rate curves were 0.870 and 0.901 for the FR and IV models, respectively, which can be interpreted as prediction accuracies of 87.00% and 90.10%, respectively (Figure 5(a)). The results indicated that the AUC values for the prediction rate curves were 0.880 and 0.923 for the FR and IV models, respectively, which can be interpreted as prediction accuracies of 88.00% and 92.30%, respectively (Figure 5(b)). The success rate and predictive rate value range between 0.8–0.9 indicate a very good performance of FR model. Also, the success rate and predictive rate value range between 0.9–1.0 implies excellent performance of the IV model.

4. Conclusion

The use of GIS and bivariate statistical models proved to be an effective approach in mapping landslide susceptibility in the Chemoga watershed, Ethiopia. The study identified several factors that influence landslide occurrences in the Chemoga watershed, such as slope, elevation, aspect, curvature, TWI, normalized difference vegetation index, road, river, land use, rainfall, and lithology. A landslide inventory map was prepared using Google earth imagery and field survey assessment. For this process, 169 landslide locations were identified and mapped. The susceptibility maps produced with the FR and IV models were divided into five susceptibility classes including very low, low, moderate, high, and very high susceptibility. The AUC rate curve quantitatively indicates the performance of the susceptibility maps. The results of this study showed that the IV model outperformed the FR model, with the accuracy of success rate 90.10% and 87.00% and the predicative rate 92.30% and 88.00%, respectively. Finally, this study confirmed that the integration of GIS and bivariate statistical models provides an effective approach in mapping landslide susceptibility in the Chemoga watershed, Ethiopia. The findings of this study can contribute to the development of a comprehensive disaster risk reduction strategy in the study area and other landslide-prone regions in Ethiopia.

Data Availability

The data used to support the findings of this study are available from the corresponding author upon request.

Conflicts of Interest

The author declares that there is no conflict of interest.

Acknowledgments

The author convey their thanks to staff of Civil Engineering Department, Debre Markos University, Ethiopia. I thanks also research square online available preprint according from the following link: https://www.researchsquare.com/article/rs-2319713/v1. This research was funded by the author.

References

[1] B. Li, N. Wang, and J. Chen, "GIS-based landslide susceptibility mapping using information, frequency ratio, and artificial neural network methods in Qinghai province, northwestern China," *Advances in Civil Engineering*, vol. 2021, Article ID 4758062, 14 pages, 2021.

[2] S. C. Pal and I. Chowdhuri, "GIS-based spatial prediction of landslide susceptibility using frequency ratio model of Lachung River basin, North Sikkim, India," *SN Applied Sciences*, vol. 1, Article ID 416, 2019.

[3] P. Gyawali, Y. M. Aryal, A. Tiwari, K. C. Prajwol, and K. Ansari, "Landslide susceptibility assessment using bivariate statistical methods: a case study of Gulmi district," *VW Engineering International*, vol. 16, no. 2, pp. 29–40, 2019.

[4] T. H. Mezughi, J. M. Akhir, A. G. Rafek, and I. Abdullah, "Landslide susceptibility assessment using frequency ratio model applied to an area along the E-W highway (Gerik-Jeli)," *American Journal of Environmental Sciences*, vol. 7, no. 1, pp. 43–50, 2011.

[5] D. M. Cruden, "A simple definition of a landslide," *Bulletin of the International Association of Engineering Geology*, vol. 43, pp. 27–29, 1991.

[6] L. Shano, T. K. Raghuvanshi, and M. Meten, "Landslide susceptibility mapping using frequency ratio model: the case of Gamo highland, South Ethiopia," *Arabian Journal of Geosciences*, vol. 14, Article ID 623, 2021.

[7] G. Mewa and F. Mengistu, "Assessment of landslide risk in Ethiopia: distributions, causes, and impacts," in *Landslides*, Y. Zhang and Q. Cheng, Eds., IntechOpen, Rijeka, 2022.

[8] C. Tesfa and K. Woldearegay, "Characteristics and susceptibility zonation of landslides in Wabe Shebelle Gorge, south eastern Ethiopia," *Journal of African Earth Sciences*, vol. 182, Article ID 104275, 2021.

[9] M. Meten, N. PrakashBhandary, and R. Yatabe, "Effect of landslide factor combinations on the prediction accuracy of landslide susceptibility maps in the Blue Nile Gorge of central Ethiopia," *Geoenvironmental Disasters*, vol. 2, Article ID 9, 2015.

[10] S. P. Mandal, A. Chakrabarty, and P. Maity, "Comparative evaluation of information value and frequency ratio in landslide susceptibility analysis along national highways of Sikkim Himalaya," *Spatial Information Research*, vol. 26, pp. 127–141, 2018.

[11] N. D. Dam, M. Amiri, N. Al-Ansari et al., "Evaluation of shannon entropy and weights of evidence models in landslide susceptibility mapping for the Pithoragarh district of Uttarakhand state, India," *Advances in Civil Engineering*, vol. 2022, Article ID 6645007, 16 pages, 2022.

[12] Z. Anis, G. Wissem, V. Vali, H. Smida, and G. Mohamed Essghaier, "GIS-based landslide susceptibility mapping using bivariate statistical methods in North-Western Tunisia," *Open Geosciences*, vol. 11, no. 1, pp. 708–726, 2019.

[13] D. Thapa and B. P. Bhandari, "GIS-based frequency ratio method for identification of potential landslide susceptible area in the Siwalik zone of Chatara-Barahakshetra section, Nepal," *Open Journal of Geology*, vol. 9, no. 12, pp. 873–896, 2019.

[14] Y.-X. Zhang, H.-X. Lan, L.-P. Li, Y.-M. Wu, J.-H. Chen, and N.-M. Tian, "Optimizing the frequency ratio method for landslide susceptibility assessment: a case study of the Caiyuan Basin in the southeast mountainous area of China," *Journal of Mountain Science*, vol. 17, pp. 340–357, 2020.

[15] T. D. Acharya, I. T. Yang, and D. H. Lee, "GIS-based landslide susceptibility mapping of Bhotang, Nepal using frequency ratio and statistical index methods," *Journal of the Korean Society of Surveying, Geodesy, Photogrammetry and Cartography*, vol. 35, no. 5, pp. 357–364, 2017.

[16] L. Li, H. Lan, C. Guo, Y. Zhang, Q. Li, and Y. Wu, "A modified frequency ratio method for landslide susceptibility assessment," *Landslides*, vol. 14, pp. 727–741, 2017.

[17] H.-J. Oh, S. Lee, and S.-M. Hong, "Landslide susceptibility assessment using frequency ratio technique with iterative random sampling," *Journal of Sensors*, vol. 2017, Article ID 3730913, 21 pages, 2017.

[18] F. E. S. Silalahi, Pamela, Y. Arifianti, and F. Hidayat, "Landslide susceptibility assessment using frequency ratio model in Bogor, West Java, Indonesia," *Geoscience Letters*, vol. 6, Article ID 10, 2019.

[19] S. Panchal and A. K. Shrivastava, "A comparative study of frequency ratio, shannon's entropy and analytic hierarchy process (AHP) models for landslide susceptibility assessment," *ISPRS International Journal of Geo-Information*, vol. 10, no. 9, Article ID 603, 2021.

[20] A. Jaafari, A. Najafi, H. R. Pourghasemi, J. Rezaeian, and A. Sattarian, "GIS-based frequency ratio and index of entropy models for landslide susceptibility assessment in the Caspian forest, northern Iran," *International Journal of Environmental Science and Technology*, vol. 11, pp. 909–926, 2014.

[21] L.-J. Wang, M. Guo, K. Sawada, J. Lin, and J. Zhang, "A comparative study of landslide susceptibility maps using logistic regression, frequency ratio, decision tree, weights of evidence and artificial neural network," *Geosciences Journal*, vol. 20, pp. 117–136, 2016.

[22] T. Melese, T. Belay, and A. Andemo, "Application of analytical hierarchal process, frequency ratio, and Shannon entropy approaches for landslide susceptibility mapping using geospatial technology: the case of Dejen district, Ethiopia," *Arabian Journal of Geosciences*, vol. 15, Article ID 424, 2022.

[23] A. Es-smairi, B. Elmoutchou, R. A. Mir, A. E. Touhami, and M. Namous, "Spatial prediction of landslide susceptibility using frequency ration (FR) and shannon entropy (SE) models : a case study from northern Rif, Morocco," *Geosystems and Geoenvironment*, pp. 1–32, 2022.

[24] L. P. Sharma, N. Patel, M. K. Ghose, and P. Debnath, "Development and application of Shannon's entropy integrated information value model for landslide susceptibility assessment and zonation in Sikkim Himalayas in India," *Natural Hazards*, vol. 75, pp. 1555–1576, 2015.

[25] N. Getachew and M. Meten, "Weights of evidence modeling for landslide susceptibility mapping of Kabi-Gebro locality, Gundomeskel area, central Ethiopia," *Geoenvironmental Disasters*, vol. 8, Article ID 6, 2021.

[26] B. Pradhan, H.-J. Oh, and M. Buchroithner, "Weights-of-evidence model applied to landslide susceptibility mapping in a tropical hilly area," *Geomatics, Natural Hazards and Risk*, vol. 1, no. 3, pp. 199–223, 2010.

[27] M. H. Rezaei Mog, M. Khayyam, M. Ahmadi, and M. Farajzadeh, "Mapping susceptibility landslide by using

the weight-of-evidence model: a case study in Merek Valley, Iran," *Journal of Applied Sciences*, vol. 7, no. 22, pp. 3342–3355, 2007.

[28] Y. Cao, X. Wei, W. Fan, Y. Nan, W. Xiong, and S. Zhang, "Landslide susceptibility assessment using the weight of evidence method: a case study in Xunyang area, China," *PLoS ONE*, vol. 16, no. 1, Article ID e0245668, 2021.

[29] S. Lee and J. Choi, "Landslide susceptibility mapping using GIS and the weight-of-evidence model," *International Journal of Geographical Information Science*, vol. 18, no. 8, pp. 789–814, 2004.

[30] Q. Wang, W. Li, W. Chen, and H. Bai, "GIS-based assessment of landslide susceptibility using certainty factor and index of entropy models for the Qianyang County of Baoji city, China," *Journal of Earth System Science*, vol. 124, pp. 1399–1415, 2015.

[31] A. Kerekes, S. L. Poszet, and A. Gál, "Landslide susceptibility assessment using the maximum entropy model in a sector of the Cluj–Napoca Municipality, Romania," *Revista de Geomorfologie*, vol. 20, no. 1, pp. 130–146, 2018.

[32] M. Shadman Roodposhti, J. Aryal, H. Shahabi, and T. Safarrad, "Fuzzy shannon entropy: a hybrid GIS-based landslide susceptibility mapping method," *Entropy*, vol. 18, no. 10, Article ID 343, 2016.

[33] A. Kornejady, M. Ownegh, and A. Bahremand, "Landslide susceptibility assessment using maximum entropy model with two different data sampling methods," *CATENA*, vol. 152, pp. 144–162, 2017.

[34] T. Mersha and M. Meten, "GIS-based landslide susceptibility mapping and assessment using bivariate statistical methods in Simada area, northwestern Ethiopia," *Geoenvironmental Disasters*, vol. 7, Article ID 20, 2020.

[35] A. Genene and M. Meten, *Landslide Susceptibility Mapping Using GIS-based Information Value and Frequency Ratio Methods in Gindeberet area, West Shewa Zone, Oromia Region*, 2021.

[36] M. Ado, K. Amitab, A. K. Maji et al., "Landslide susceptibility mapping using machine learning: a literature survey," *Remote Sensing*, vol. 14, no. 13, Article ID 3029, 2022.

[37] F. S. Tehrani, M. Calvello, Z. Liu, L. Zhang, and S. Lacasse, "Machine learning and landslide studies: recent advances and applications," *Natural Hazards*, vol. 114, pp. 1197–1245, 2022.

[38] M. Azarafza, M. Azarafza, H. Akgün, P. M. Atkinson, and R. Derakhshani, "Deep learning-based landslide susceptibility mapping," *Scientific Reports*, vol. 11, Article ID 24112, 2021.

[39] J. M. Habumugisha, N. Chen, M. Rahman et al., "Landslide susceptibility mapping with deep learning algorithms," *Sustainability*, vol. 14, no. 3, Article ID 1734, 2022.

[40] T. C. Korma, "GIS-based landslide susceptibility zonation mapping using frequency ratio and logistics regression models in the Dessie area, South Wello, Ethiopia," pp. 1–25, 2022.

[41] K. Solaimani, S. Z. Mousavi, and A. Kavian, "Landslide susceptibility mapping based on frequency ratio and logistic regression models," *Arabian Journal of Geosciences*, vol. 6, pp. 2557–2569, 2013.

[42] S. Hidayat, H. Pachri, and I. Alimuddin, "Analysis of landslide susceptibility zone using frequency ratio and logistic regression method in Hambalang, Citeureup district, Bogor Regency, West Java province," *IOP Conference Series: Earth and Environmental Science*, vol. 280, Article ID 012005, 2019.

[43] S. Lee and B. Pradhan, "Landslide hazard mapping at Selangor, Malaysia using frequency ratio and logistic regression models," *Landslides*, vol. 4, pp. 33–41, 2007.

[44] G. Das and K. Lepcha, "Application of logistic regression (LR) and frequency ratio (FR) models for landslide susceptibility mapping in Relli Khola river basin of Darjeeling Himalaya, India," *SN Applied Sciences*, vol. 1, Article ID 1453, 2019.

[45] C. Sivakami and R. Rajkumar, "Landslide vulnerability zone by weights of evidence model using remote sensing and GIS, in Kodaikanal Taluk (Tamil Nadu, India)," *International Journal of Engineering Research & Technology (IJERT)*, vol. 9, no. 2, pp. 788–793, 2020.

[46] A. Wubalem, "Modeling of landslide susceptibility in a part of Abay Basin, northwestern Ethiopia," *Open Geosciences*, vol. 12, no. 1, pp. 1440–1467, 2020.

[47] B. Pradhan, S. Lee, and M. F. Buchroithner, "Remote sensing and GIS-based landslide susceptibility analysis and its cross-validation in three test areas using a frequency ratio model," *Photogrammetrie—Fernerkundung —Geoinformation*, vol. 2010, no. 1, pp. 17–32, 2010.

[48] A. Wubalem, "Landslide susceptibility mapping using statistical methods in Uatzau catchment area, northwestern Ethiopia," *Geoenvironmental Disasters*, vol. 8, Article ID 1, 2021.

[49] L. Ayalew and H. Yamagishi, "The application of GIS-based logistic regression for landslide susceptibility mapping in the Kakuda-Yahiko Mountains, central Japan," *Geomorphology*, vol. 65, no. 1-2, pp. 15–31, 2005.

[50] G.-L. Du, Y.-S. Zhang, J. Iqbal, Z.-H. Yang, and X. Yao, "Landslide susceptibility mapping using an integrated model of information value method and logistic regression in the Bailongjiang watershed, Gansu province, China," *Journal of Mountain Science*, vol. 14, pp. 249–268, 2017.

[51] B. T. Pham, D. T. Bui, M. B. Dholakia et al., "A novel ensemble classifier of rotation forest and naïve bayer for landslide susceptibility assessment at the Luc Yen district, Yen Bai province (Viet Nam) using GIS," *Geomatics, Natural Hazards and Risk*, vol. 8, no. 2, pp. 649–671, 2017.

[52] C. Xu, F. Dai, X. Xu, and Y. H. Lee, "GIS-based support vector machine modeling of earthquake-triggered landslide susceptibility in the Jianjiang River watershed, China," *Geomorphology*, vol. 145-146, pp. 70–80, 2012.

[53] H. Shu, Z. Guo, S. Qi, D. Song, H. R. Pourghasemi, and J. Ma, "Integrating landslide typology with weighted frequency ratio model for landslide susceptibility mapping: a case study from Lanzhou city of northwestern China," *Remote Sensing*, vol. 13, no. 18, Article ID 3623, 2021.

[54] S. He, P. Pan, L. Dai, H. Wang, and J. Liu, "Application of kernel-based fisher discriminant analysis to map landslide susceptibility in the Qinggan River delta, Three Gorges, China," *Geomorphology*, vol. 171-172, pp. 30–41, 2012.

[55] H. Khan, M. Shafique, M. A. Khan, M. A. Bacha, S. U. Shah, and C. Calligaris, "Landslide susceptibility assessment using frequency ratio, a case study of northern Pakistan," *The Egyptian Journal of Remote Sensing and Space Science*, vol. 22, no. 1, pp. 11–24, 2019.

[56] N. R. Regmi, J. R. Giardino, and J. D. Vitek, "Modeling susceptibility to landslides using the weight of evidence approach: Western Colorado, USA," *Geomorphology*, vol. 115, no. 1-2, pp. 172–187, 2010.

[57] C.-Y. Chen and F.-C. Yu, "Morphometric analysis of debris flows and their source areas using GIS," *Geomorphology*, vol. 129, no. 3-4, pp. 387–397, 2011.

[58] D. Sarkar, S. Saha, and P. Mondal, "GIS-based frequency ratio and Shannon's entropy techniques for flood vulnerability assessment in Patna district, central Bihar, India," *International Journal of*

Environmental Science and Technology, vol. 19, pp. 8911–8932, 2022.

[59] S. Lee and J. A. Talib, "Probabilistic landslide susceptibility and factor effect analysis," *Environmental Geology*, vol. 47, pp. 982–990, 2005.

[60] A. D. Regmi, K. Yoshida, H. R. Pourghasemi, M. R. DhitaL, and B. Pradhan, "Landslide susceptibility mapping along Bhalubang —Shiwapur area of mid-western Nepal using frequency ratio and conditional probability models," *Journal of Mountain Science*, vol. 11, pp. 1266–1285, 2014.

[61] S. Karim, S. Jalileddin, and M. T. Ali, "Zoning landslide by use of frequency ratio method (case study: Deylaman region)," *Middle-East Journal of Scientific Research*, vol. 9, no. 5, pp. 578–583, 2011.

[62] F. Guzzetti, "Landslide hazard assessment and risk evaluation: limits and prospectives," in *Proceedings of the 4th EGS Plinius Conference held at Mallorca, Spain, October 2002*, pp. 1–4, 2003.

[63] E. Yesilnacar and T. Topal, "Landslide susceptibility mapping: a comparison of logistic regression and neural networks methods in a medium scale study, Hendek region (Turkey)," *Engineering Geology*, vol. 79, no. 3-4, pp. 251–266, 2005.

[64] T. Fawcett, "An introduction to ROC analysis," *Pattern Recognition Letters*, vol. 27, no. 8, pp. 861–874, 2006.

[65] S. Mohsen Mousavi, A. Golkarian, S. Amir Naghibi, B. Kalantar, and B. Pradhan, "GIS-based groundwater spring potential mapping using data mining boosted regression tree and probabilistic frequency ratio models in Iran," *AIMS Geosciences*, vol. 3, no. 1, pp. 91–115, 2017.

[66] A. Haghizadeh, S. Siahkamari, A. H. Haghiabi, and O. Rahmati, "Forecasting flood-prone areas using Shannon's entropy model," *Journal of Earth System Science*, vol. 126, Article ID 39, 2017.